PCCP

Reduction of Np(VI) with Hydrazinopropionitrile via Water-mediated Proton Transfer

Journal:	*Physical Chemistry Chemical Physics*
Manuscript ID	CP-PER-04-2022-001730.R2
Article Type:	Paper
Date Submitted by the Author:	05-Jul-2022

Complete List of Authors:	Li, Xiao-Bo; Institute of High Energy Physics Chinese Academy of Sciences Wu, Qun-Yan; Institute of High Energy Physics Chinese Academy of Sciences, Wang, Congzhi; Institute of High Energy Physics Chinese Academy of Sciences, Laboratory of Nuclear Energy Chemistry Lan, Jianhui; Institute of High Energy Physics Chinese Academy of Sciences, Laboratory of Nuclear Energy Chemistry Zhang, Meng; Harbin Engineering University, College of Nuclear Science and Technology Gibson, John; Lawrence Berkeley National Laboratory, Chemical Sciences Division Chai, Zhifang; Institute of High Energy Physics Chinese Academy of Sciences Shi, Weiqun; Institute of High Energy Physics Chinese Academy of Sciences

Reduction of Np(VI) with Hydrazinopropionitrile via Water-mediated Proton Transfer

Xiao-Bo Li, [†,‡] Qun-Yan Wu,*[,†] Cong-Zhi Wang, [†] Jian-Hui Lan, [†] Meng Zhang, [‡]

John K. Gibson, [&] Zhi-Fang Chai, [†] and Wei-Qun Shi*[,†]

[†]Laboratory of Nuclear Energy Chemistry, Institute of High Energy Physics, Chinese Academy of Sciences, Beijing 100049, China

[‡]Fundamental Science on Nuclear Safety and Simulation Technology Laboratory, College of Nuclear Science and Technology, Harbin Engineering University, Harbin, Heilongjiang, 150001, China

[&]Chemical Sciences Division, Lawrence Berkeley National Laboratory, Berkeley, California, 94720, USA

Email: wuqy@ihep.ac.cn, shiwq@ihep.ac.cn

*To whom correspondence should be addressed

Abstract

Effectively adjusting and controlling the valence state of neptunium (Np) is essential in its separation during spent fuel reprocessing. Hydrazine and its derivatives as free-salts can selectively reduce Np(VI) to Np(V). Reduction mechanisms of Np(VI) with hydrazine and four derivatives have been explored using multiple theoretical methods in our previous works. Herein, we examine the reduction mechanism of Np(VI) with hydrazinopropionitrile ($NCCH_2N_2H_3$) which exhibits faster kinetics than most other hydrazine derivatives probably due to its σ-π hyperconjugation effect. Free radical ion pathways I, II and III involving the three types of hydrazine H atoms were found that correspond to the experimentally established mechanism of reduction of two Np(VI) via initial oxidation to $[NCCH_2N_2H_3]^{+\bullet}$, followed by conversion to $NCCH_2N_2H$ (+ $2H_3O^+$) and ultimately to CH_3CN + N_2. Potential energy profiles suggest that the second redox stage is rate-determining for all three pathways. Pathway I with water-mediated proton transfer is energetically preferred for hydrazinopropionitrile. Analyses using the approaches of localized molecular orbitals (LMOs), quantum theory of atoms in molecules (QTAIM), and intrinsic reaction coordinate (IRC) elucidate the bonding evolution for the structures on the reaction pathways. The results of the spin density reveal that the reduction of the first Np(VI) ion is the outer-sphere electron transfer, while that of the second Np(VI) ion is the hydrogen transfer. This work offers new insights into the nature of reduction of Np(VI) by hydrazinopropionitrile via water-mediated proton transfer, and provides a basis for designing free-salt reductants for Np separations.

Introduction

Neptunium-237 (^{237}Np) is synthesized by neutron irradiation of uranium (U). As a by-product of irradiation of ^{235}U based fuels in conventional nuclear reactors it appears in waste streams of the industrial PUREX (Plutonium Uranium Reduction Extraction) process.[1, 2] Generally, about 60% of neptunium is co-extracted with uranium and plutonium in the first PUREX extraction stage, with the remainder entering the highly radioactive waste stream. Control of neptunium significantly increases the complexity and waste volumes of the PUREX process.[3] As neptunium-237 is a useful resource, including as the target material for ^{238}Pu production, its recovery is highly desirable. In the PUREX process Np(VI), Pu(IV) and U(VI) in the aqueous phase are extracted together into the organic phase by the extractant tributyl phosphate (TBP). Moreover, the extraction ability of TBP for three oxidation states of Np follows the order of Np(VI) > Np(IV) >> Np(V). Therefore, the more efficient separation of Np from U and Pu in the PUREX process is the reduction of Np(VI) to Np(V). Experimental results have been reported for several highly efficient and environment-friendly Np(VI) reductants, including oximes,[4-6] aldehydes,[7-9] hydroxylamine,[10-14] urea,[15, 16] hydroxamic acid,[17-20] hydrazine,[21-28] and their derivatives. Acetaldoxime reduces Np(VI) to Np(V) only at less than 2 M nitric acid concentration and low temperature (308 K).[4] Uchiyama *et al*. proposed a novel Np/Pu/U separation process using *n*- and *iso*-butyraldehydes taking advantage of different reduction abilities,[7] with *n*-butyraldehyde reducing Np(VI) to Np(V), but not Pu(IV) or U(VI). It has been shown that reduction of Np(VI) by *N*,*N*-ethyl (hydroxyethyl) hydroxylamine is faster than by *N*,*N*-diethyl hydroxylamine.[10] Dihydroxyurea is sometimes used as a stripping agent for separating Np because it quickly reduces Np(VI) to Np(V), but only inefficiently further reduces Np(V) to Np(IV).[16] Taylor and co-workers reported that formo- and aceto-hydroxamic acids effectively reduce Np(VI) to Np(V) for separation of Np from U.[17]

Reduction kinetics and mechanisms of Np(VI)-to-Np(V) reduction by hydrazine and its derivatives have been extensively studied, because they do not reduce Pu(IV) and U(VI) under properly controlled conditions.[22, 24] Marchenko *et al*. reported that the

reaction rates of Np(VI) with most hydrazine derivatives is greater than with hydrazine, with particularly fast kinetics for hydrazinopropionitrile (HzPn),[26] a distinction that motivated the present theoretical investigation. There are many theoretical works on reaction mechanisms for reduction processes involving main group, transition metal, and rare earth metals,[29-33] but relatively few for actinides, largely due to their complex electronic structures.[34-40]

We previously theoretically investigated the reduction mechanism of Np(VI) with hydrazine,[41] 2-hydroxyethyl-, methyl-, formylhydrazine,[42] and phenylhydrazine.[43] Here we report results for reduction of Np(VI) by HzPn via a water-mediated proton transfer. Water-assisted proton transfer plays an essential role in lowering the reaction energy barrier in systems containing phosphotungstic acid,[44] amino acids,[45-47] and nucleic acid bases.[48] However, reports of reactions with water-assisted proton transfer are sparse for metal-bearing systems,[49-53] especially actinide metals. The mechanism identified here for Np(VI) reduction with HzPn involves a remarkable water-mediated proton transfer, which may contribute to further advances in separations of Np from U and Pu in spent fuel reprocessing.

Computational Methods

Mechanisms for the reaction of Np(VI) with HzPn were studied using the hybrid B3LYP exchange-correlation functional[54, 55] within the Gaussian16 program,[56] as used previously in calculations of actinide complexes.[57-61] We used the non-relativistic Hamiltonian for the integral calculations, of which the relativistic effect is taken into consideration via the relativistic effective core potential and the corresponding basis sets. The relativistic effective core potential (RECP)[62] using the 60 core electrons together with the ECP60MWB-SEG valence basis set[63, 64] were employed for Np; the 6-31G(d) basis set was applied to O, N, C, and H. The structures of stationary points for the potential energy profiles (PEPs) were optimized at the B3LYP/ECP60MWB/6-31G(d) level of theory. The solvation model density (SMD) was used to simulate the aqueous environment. Gibbs free energies were used for the reported PEPs. The triplet state of the $[NpO_2(H_2O)_5]^+$ is confirmed to be the

ground state in previous study,[65] so all Np(VI) and Np(V) complexes were treated with doublet and triplet spin as ground states, respectively, using the spin-unrestricted method. Calculations of harmonic vibrational frequencies were performed to ensure positive values for optimized structures of all initial complexes (ICs) and intermediates (INTs). Each transition state (TS) was confirmed to have a sole imaginary frequency. The reaction pathways were further evaluated by intrinsic reaction coordinate (IRC) calculations.[66] The quantum theory of atoms in molecules (QTAIM) method[67, 68] and the localized molecular orbitals (LMOs)[69] were employed to evaluate bonding evolution using the Multiwfn code.[70] Referenced atom labels for neutral and ionized HzPn are shown in Scheme 1.

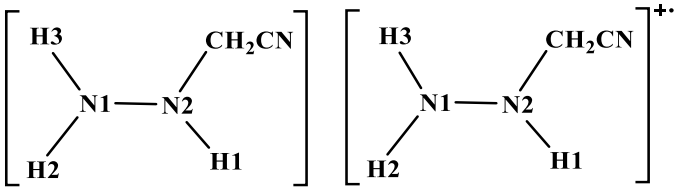

Scheme 1 Atom numbering for neutral and ionized HzPn.

Results and Discussion

The overall reduction of $[Np^{VI}O_2(H_2O)_5]^{2+}$ by HzPn in aqueous phase is given by eqn (1) based on reported experimental results.[21, 23] The speculated reaction mechanism is shown by eqns (2)-(4).

$2[Np^{VI}O_2(H_2O)_5]^{2+} + NCCH_2N_2H_3 + 2H_2O = 2[Np^{V}O_2(H_2O)_5]^{+} + CH_3CN + N_2 + 2H_3O^{+}$ (1)

$[Np^{VI}O_2(H_2O)_5]^{2+} + NCCH_2N_2H_3 \rightarrow [Np^{V}O_2(H_2O)_5]^{+} + [NCCH_2N_2H_3]^{+\bullet}$ (2)

$[Np^{VI}O_2(H_2O)_5]^{2+} + [NCCH_2N_2H_3]^{+\bullet} + 2H_2O \rightarrow [Np^{V}O_2(H_2O)_5]^{+} + NCCH_2N_2H + 2H_3O^{+}$ (3)

$NCCH_2N_2H \rightarrow CH_3CN + N_2$ (4)

Reduction of Np(VI) to Np(V) according to stages given by eqns (2) (first stage) and (3) (second stage) can occur via reaction pathways I, II, and III corresponding to direct participation of the three hydrazino hydrogens, H1, H2, and H3 identified in

Scheme 1 for $NCCH_2N_2H_3$ and $[NCCH_2N_2H_3]^{+\bullet}$. The lowest unoccupied molecular orbital (LUMO) and the high occupied molecular orbitals (HOMOs) of $NCCH_2N_2H_3$ and $[NCCH_2N_2H_3]^{+\bullet}$ are displayed in Figs. S1 and S2, respectively. It shows that the HOMO-5 exists σ-π hyperconjugation effect owing to σ electron in C_{alkyl}-H and π electron in cyano group, which has a weak electron-donating ability.

Reaction Pathways. The PEPs for pathways I, II and III based on Gibbs free energy in Fig. 1 describe the mechanism of the entire reaction. It is apparent there that the energy barrier from the IC to TS is significantly higher for the second reduction stage versus the first for all three pathways, suggesting the second stage is rate-determining. Pathway I has a14.36 kcal mol^{-1} energy barrier from $IC3^I$ to $TS3^I$, whereas the corresponding barriers for pathways II and III are comparable, at 18.57 and 18.28 kcal mol^{-1}, respectively, where these comparable values reflect participation of similar atoms H2 and H3. The lower barrier for pathway I point to it as the preferred mechanism, probably due to the water-mediated proton transfer discussed below. The Gibbs free energy for eqn (1) of -69.16 kcal mol^{-1} indicates thermodynamically quite favorable reduction of Np(VI) to Np(V) by HzPn. The results obtained here are rather different from previously reported mechanisms for hydrazine,[41] formyl hydrazine, methyl hydrazine, 2-hydroxyethyl hydrazine,[42]and phenylhydrazine.[43] In particular, only a free radical ion mechanism was found for reduction of Np(VI) with HzPn, whereas both free radical ion and free radical mechanisms were identified for the other hydrazine derivatives.[42, 43] The computed energy barrier for the second stage of reduction by HzPn (14.36 kcal mol^{-1}) is lower than for 2-hydroxyethyl hydrazine (15.15 kcal mol^{-1}), methyl hydrazine (16.57 kcal mol^{-1}) and formyl hydrazine (22.81 kcal mol^{-1}),[42] whereas it is higher than for phenylhydrazine (12.89 kcal mol^{-1}),[43] which is consistent with experimental results.[71] These comparisons suggest that HzPn shows better reduction ability than most other hydrazine derivatives, probably due to the σ-π hyperconjugation effect, which is similar with phenylhydrazine with a weak electron-donating group. So it is concluded that the hydrazine derivatives with a weak electron-donating group can lower the energy barrier of the reaction.

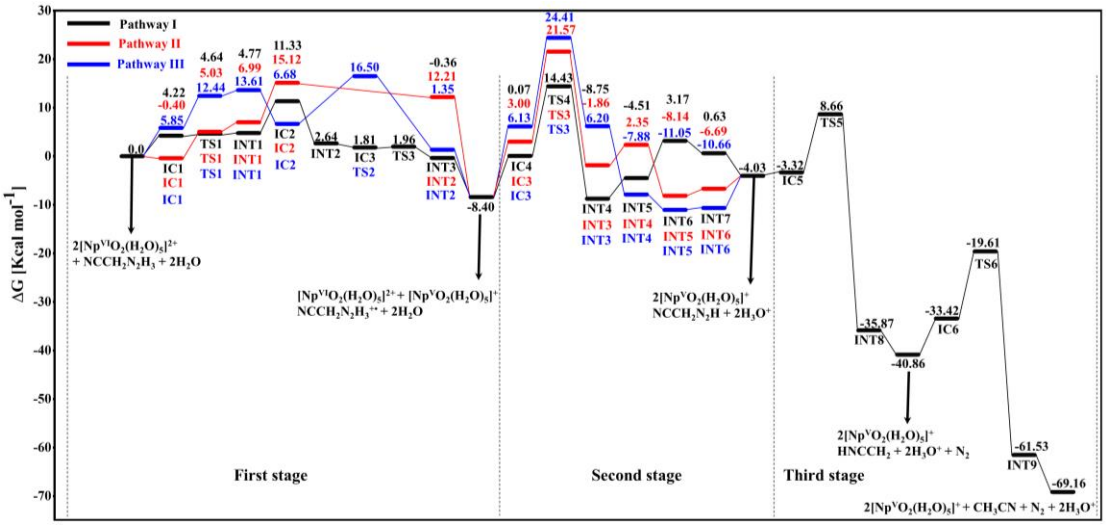

Fig. 1 Potential energy profiles for the reduction of two Np(VI) by one hydrazinopropionitrile at the B3LYP/ECP60MWB/6-31G(d) level of theory.

According to the PEPs in Fig. 1, we elucidate the structures and mechanisms of the three stages for the most favorable pathway I in Figs. 2-4. In the first stage of pathway I depicted in Fig. 2, the transformation from $IC1^I$ to $INT1^I$ is endothermic by 0.55 kcal mol^{-1}, which is slightly higher than the 0.42 kcal mol^{-1} barrier from $IC1^I$ to $TS1^I$. Notably, the $TS1^I$ barrier for the first stage with HzPn is significantly lower than reported for other hydrazine derivatives with Np(VI).[42, 43] Although the $INT1^I$ is predicted to be very slightly higher in Gibbs free energy than $TS1^I$, it is lower in electronic energy (Table S1 of SI). The N2-H1 bond distance elongates from 1.057 in $IC1^I$ to 1.341 in $TS1^I$ to 1.721 Å in $INT1^I$, while the O_{yl1}-H1 distance concurrently decreases from 1.669 in $IC1^I$ to 1.165 in $TS1^I$ to 1.021 Å in $INT1^I$. Dissociation of the N2-H1 bond in $NCCH_2N_2H_3$ and formation of the O_{yl1}-H1 bond in $INT1^I$ is confirmed by imaginary frequency 800.52i cm^{-1} for the N2-H1-O_{yl1} vibrational mode in $TS1^I$. Transfer of H1 to O_{yl1} is accompanied by an increase in the Np-O_{yl1} bond distance from 1.870 in $IC1^I$, to 1.944 in $TS1^I$, to 2.002 Å in $INT1^I$, and a decrease in the Np-O_{yl2} bond distance from 1.835 to 1.819 to 1.812 Å. For $IC1^I$, $TS1^I$, and $INT1^I$ there are five waters coordinated in the neptunyl equatorial plane, with one forming a hydrogen bond to the nitrile with N-H distance ~2.0 Å. Initial formation of $IC2^I$ from $INT1^I$ by adding a water molecule is an endoergic by 6.56 kcal mol^{-1}. For the structures from $IC2^I$ to $INT3^I$, another water molecule can assist double-proton

transfer, which easily achieve inter-molecular proton transfer. There are five hydrogen bonds in $IC2^I$ involving water molecules, along with a short O_{yl1}-H1 bond distance of 1.040 Å. Subsequent dissociation of this O_{yl1}-H1 bond is accompanied by its elongation to 1.607 Å in $INT2^I$ with exothermicity -8.69 kcal mol^{-1} relative to $IC2^I$, with the result a coordinated H_3O^+ in $INT2^I$ after proton-transfer from O_{yl1}-H1. A slight structural change occurs around the H_3O^+ moiety from $INT2^I$ to $IC3^I$, as emphasized in the red circle in Fig. 2. After $IC3^I$, hydrogen H_w of H_3O^+ is transferred to N2 via $TS3^I$ with imaginary frequency 730.94i cm^{-1}, which presents barrier of only 0.15 kcal mol^{-1}. From $IC3^I$ to $INT3^I$ the O_w-H_w distance increases by 0.502 Å while N2-H_w decreases by 0.520 Å. Besides, from $IC2^I$ to $INT3^I$, Np-O_{yl1} bond consistently shortens and Np-O_{yl2} bond vice versa, which is different from $IC1^I$ to $INT1^I$. The Gibbs free energy change for eqn (2) is favorable, -8.40 kcal mol^{-1}. This first stage terminates with $INT3^I$ dissociating into $[Np^VO_2(H_2O)_5]^+$, H_2O, and free radical ion $[NCCH_2N_2H_3]^{+\bullet}$ which serves as the reductant in the second stage, eqn (3). Such radical ions of hydrazine derivatives in reduction processes have previously been identified by electron paramagnetic resonance spectroscopy.[72]

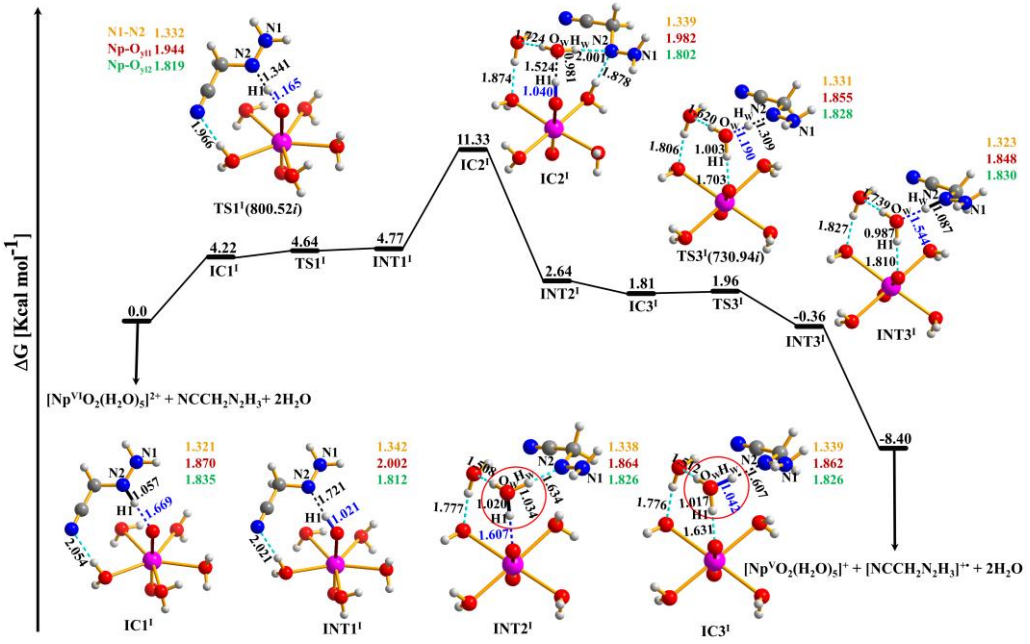

Fig. 2 PEPs and structures for the first stage of pathway I at the B3LYP/ECP60MWB/6-31G(d) level of theory. Values in parentheses are TS imaginary frequencies (cm^{-1}). O_{yl1} and O_{yl2} represent neptunyl oxygen atom that is involved or not involved in bonding, respectively.

The PEP for the second stage of pathway I, eqn 3, is shown in Fig. 3. Starting with $IC4^I$, H1 bound to N2 in $[NCCH_2N_2H_3]^{+\bullet}$ is transferred to O_{yl1} via $TS4^I$ with imaginary frequency 1309.69i cm^{-1} that corresponds to stretching vibrations of H1 between N2 and O_{yl1}, and H2 between N1 and O_w. The transformation $IC4^I \rightarrow INT4^I$ is exothermic by -8.82 kcal mol^{-1}, via the 14.36 kcal mol^{-1} barrier from $IC4^I$ to $TS4^I$. The N2-H1 and O_{yl1}-H1 bond distances change moderately from $IC4^I$ to $TS4^I$, but more drastically from $TS4^I$ to $INT4^I$ in which there is essentially no N2-H1 bond and a short O_{yl1}-H1 bond with distance 0.984 Å. In contrast to the five inner-sphere coordinating water molecules in $IC1^I$, $TS1^I$ and $INT1^I$ in the first stage, only three waters strongly coordinated to neptunyl in $IC4^I$, $TS4^I$ and $INT4^I$. One of the non-coordinated waters forms hydrogen bonds with two coordinated waters, with O-H distances of ~1.7 and ~1.9 Å, while the other is weakly coordinating to Np and hydrogen bonded with H2. The N1-H2 bond distance increases drastically, from 1.041 Å in $IC4^I$ to 1.539 Å in $TS4^I$, and then decreases to 1.088 Å in $INT4^I$; the O_w-H2 distance coincidentally decreases from 1.773 Å in $IC4^I$ to 1.066 Å in $TS4^I$, then increasing to 1.554 Å in $INT4^I$. Notably, these bond distance changes reveal that N1-H2 bonding is similar in $IC4^I$ and $INT4^I$, with its disruption and elongation in $TS4^I$ facilitating transfer of H1 from N2 to O_{yl1}, this phenomenon is characterized as water-mediated proton transfer, which is not found in the first Np(VI) reduction by $NCCH_2N_2H_3$, probably attribute to the easier proton donation of $[NCCH_2N_2H_3]^{+\bullet}$. Transfer of H1 to O_{yl1} is accompanied by the Np-O_{yl1} bond distance increasing from 1.755 Å in $IC4^I$, to 1.805 Å in $TS4^I$, and to 2.037 Å in $INT4^I$. The N1-N2 distance decreases from 1.321 in $IC4^I$, to 1.268 in $TS4^I$, and to 1.229 Å in $INT4^I$, which is the opposite of the trend in the first stage from $IC1^I$ to $INT1^I$. This disparity between the stages indicates that removal of H1 from the neutral molecule in the first stage weakens and elongates the N1-N2 bond, whereas removal from the radical cation in stage two strengthens and shortens it. Transfer of H1 atom from N2 of $[NCCH_2N_2H_3]^{+\bullet}$ to O_{yl1} realizes the Np(VI) reduction. Addition of two water molecules to $INT4^I$ yields $INT5^I$ based on the stoichiometry of eqn (3). The N1-H3 bond is drastically elongated, from 1.080 Å in $INT5^I$ to 1.629 Å in $INT6^I$, and the

O_{yl1}-H1 bond is disrupted from INT6^{I} to INT7^{I}, with its distance increasing from 1.041 to 1.790 Å. This result reveals that dissociation of the O_{yl1}-H1 bond proceeds via water-terminated proton transfer. Finally, INT7^{I} dissociates into $[Np^{V}O_2(H_2O)_5]^{+}$, $2H_3O^{+}$, and intermediate $NCCH_2N_2H$. As shown in Fig. 3, the Gibbs free energy change for eqn (3) is -4.10 kcal mol^{-1}; this stage of the reduction process is both kinetically and thermodynamically accessible. In addition, some Np-O_w bonds are significantly longer, which leads to coordinated water molecules deviated from the Np atom and forms more hydrogen bonds.

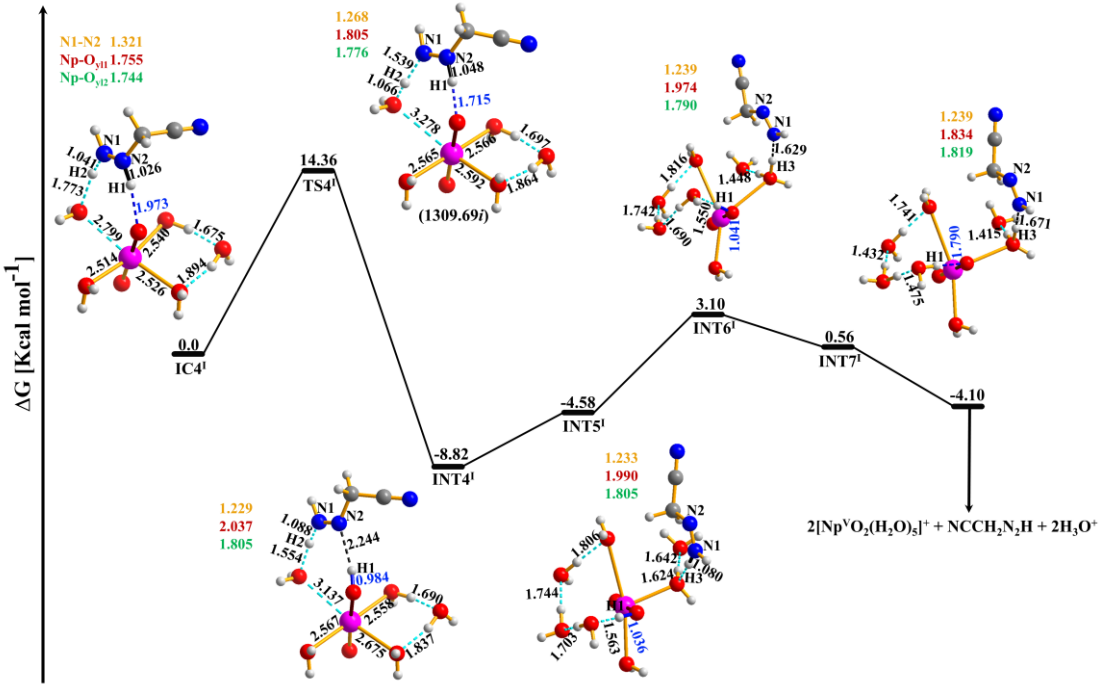

Fig. 3 PEPs and structures for the second stage of pathway I at the B3LYP/ECP60MWB/6-31G(d) level of theory. Values in parentheses are TS imaginary frequencies (cm^{-1}).

The third stage of pathway I is decomposition of intermediate $NCCH_2N_2H$ to stable N_2 and CH_3CN via the PEP in Fig. 4. Firstly, there is intramolecular hydrogen transfer in which H2 of $NCCH_2N_2H$ contacts the cyano N atom via TS5^{I} with energy barrier of 11.98 kcal mol^{-1}, which forms N_2 and ketenimine CH_2CNH. Secondly, CH_2CNH is isomerized to more stable CH_3CN. The isomerization barrier was evaluated for 0-2 water molecules as shown in Fig. S3, where it was found that specifically two waters greatly facilitate proton transfer with the isomerization barrier decreasing from 62.66

kcal mol^{-1} without waters to 13.82 kcal mol^{-1} with two, via TS6^{I} with imaginary frequency 313.68i cm^{-1} (Fig. 4). This result is supported by the report in previous studies that water-assisted proton transfer can reduce the reaction energy barrier.[44-48]

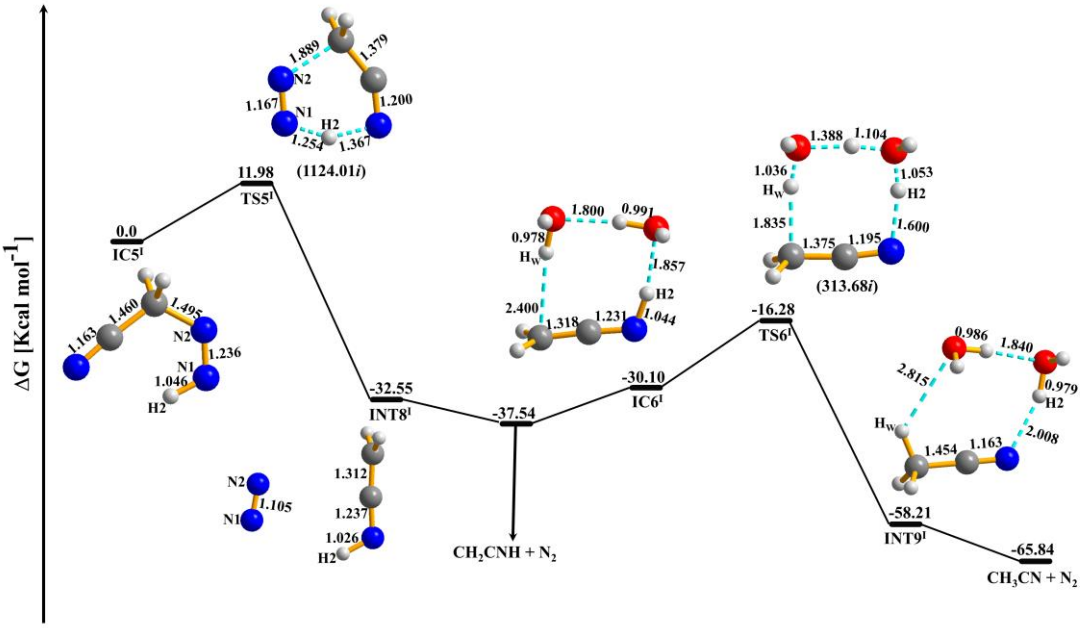

Fig. 4 PEPs and structures for the third stage of pathway I at the B3LYP/ECP60MWB/6-31G(d) level of theory. Values in parentheses are TS imaginary frequencies (cm^{-1}).

In pathway I there is initial association of H1 to O_{yl1} with both reductants, $NCCH_2N_2H_3$ and $[NCCH_2N_2H_3]^{+\bullet}$, while for pathways II and III this initial association to O_{yl1} is by H2 and H3, respectively. The PEPs, optimized structures of five TSs, and imaginary frequencies for pathways II and III are in Fig. 5, with the IC and INT structures in Figs. S4 and S5. In pathway II, the first stage is dissociation of the N1-H2 bond in IC1^{II}, resulting in formation of the O_{yl1}-H2 bond in INT1^{II} via TS1^{II} with energy barrier 5.43 kcal mol^{-1}. IC2^{II} is the complex of INT1^{II} and one water molecule. Dissociation of the O_{yl1}-H2 bond in IC2^{II} and formation of the N1-H_w bond in INT2^{II} are enable by a water (Fig. S4), corresponding to slightly exothermic (-2.91 kcal mol^{-1}) water-assisted double-proton transfer from IC2^{II} to INT2^{II}. Like INT3^{I} in pathway I, INT2^{II} dissociates into $[Np^{V}O_2(H_2O)_5]^{+}$, H_2O, and free radical ion $[NCCH_2N_2H_3]^{+\bullet}$. In the second stage of pathway II, transfer of H2 from $[NCCH_2N_2H_3]^{+\bullet}$ to O_{yl1} occurs via TS3^{II} with imaginary frequency 4270.71i cm^{-1}.

$INT3^{II}$ is complexed by two waters to yield $INT4^{II}$, with the N2-H1 bond cleaved to yield $INT5^{II}$, and the O_{yl1}-H2 bond cleaved to yield $INT6^{II}$ (Fig. S4). This sequence corresponds to dissociation of the O_{yl1}-H2 bond via water- terminated proton transfer. Finally, $INT6^{II}$ dissociates to $[Np^{V}O_2(H_2O)_5]^+$, $2H_3O^+$, and $NCCH_2N_2H$.

In the first stage of pathway III, the H3 atom of $NCCH_2N_2H_3$ contacts O_{yl1} via $TS1^{III}$ with barrier 6.59 kcal mol^{-1}, which is 6.17 kcal mol^{-1} higher than $TS1^{I}$, indicating significantly more facile transfer of H1 versus H3. $IC2^{III}$ is the complex of $INT1^{III}$ and one water molecule, which is exothermic by 6.93 kcal mol^{-1}. Dissociation of the O_{yl1}-H3 bond in $IC2^{III}$, and formation of N1-H_w bond in $INT2^{III}$ occurs via $TS2^{III}$ with energy barrier 9.82 kcal mol^{-1}, with the process again corresponding to water-assisted double-proton transfer. To complete the first stage, $INT2^{III}$ dissociates into $[Np^{V}O_2(H_2O)_5]^+$, H_2O, and $[NCCH_2N_2H_3]^{+\bullet}$. In the second stage, H3 in $[NCCH_2N_2H_3]^{+\bullet}$ is transferred to O_{yl1} via $TS3^{III}$ with barrier 18.28 kcal mol^{-1}, which is 3.93 kcal mol^{-1} higher than the corresponding pathway I barrier, while 0.29 kcal mol^{-1} lower than for pathway II. $INT4^{III}$, the complex of $INT3^{III}$ and two waters, converts to $INT6^{III}$ via cleavage of bonds N2-H1 and O_{yl1}-H3 assisted by two waters that are converted to H_3O^+ ions in $INT6^{III}$. Finally, $INT6^{III}$ dissociates into $[Np^{V}O_2(H_2O)_5]^+$, $2H_3O^+$, and $NCCH_2N_2H$. As noted above, the three alternative reductant H1, H2 and H3 atoms participate in the different mechanisms given by pathways I, II and III, respectively. Water-mediated proton transfer processes occur for all three pathways; for pathway I it results in the lowest rate-determining energy barrier of the three.

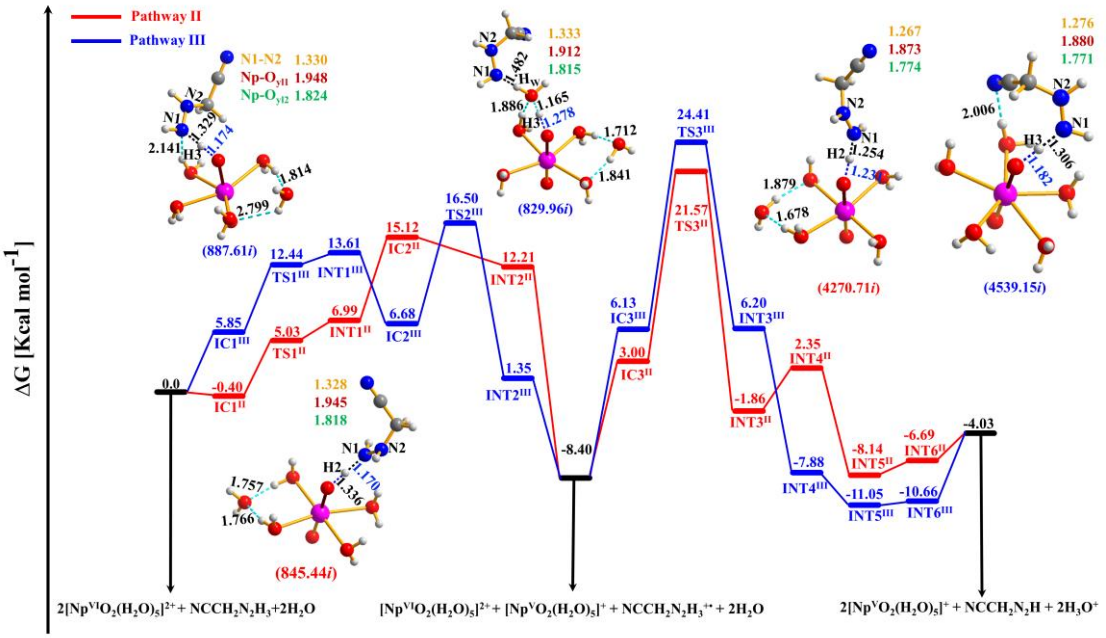

Fig. 5 PEPs and TS structures (and imaginary frequencies in cm^{-1}) for pathways II and III at the B3LYP/ECP60MWB/6-31G(d) level of theory.

IRC Analysis. IRC calculations were performed to verify that TS structures connect with reactants and products. IRC results for $TS4^{I}$ connecting $IC4^{I}$ and $INT4^{I}$ are in Fig. 6, with results for other TSs on all three pathways in Figs. S6-S16. In Fig. 6, the distance of the N2-H1 bond slightly changes from structure **1** (1.025 Å) to $TS4^{I}$ (1.048 Å), whereas the N1-H2 bond concurrently increases more substantially, from 1.041 to 1.539 Å. From $TS4^{I}$ to structure **8**, the N2-H1 bond elongates drastically, from 1.048 to 2.146 Å. The N1-H2 bond elongates from 1.539 Å in $TS4^{I}$ to 1.672 Å in structure **5**, then contracts to 1.088 Å in **8**. The result that the N1-H2 bond first weakens before strengthening reveals facilitation of H1 transfer from N2 to O_{yl1}, to wit water-mediated proton transfer.

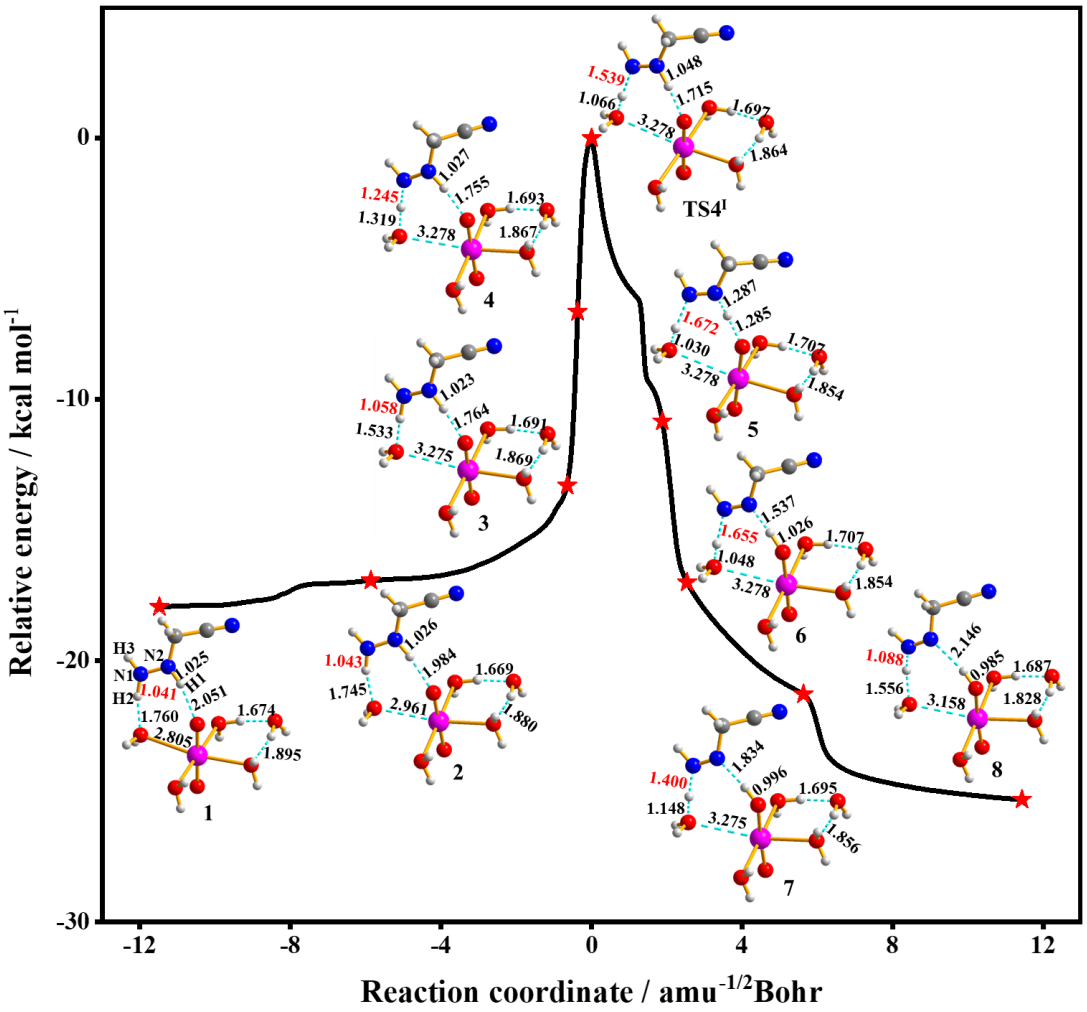

Fig. 6 IRC for TS4^{I} showing selected structures along the IRC.

QTAIM and MBO. Topology analysis based on Bader's QTAIM[68, 73] has been applied to dissect dissociation and formation of chemical bonds.[74, 75] The electron density [ρ(r)] and its Laplacian [$\nabla^2\rho$(r)] at the bond critical point (BCP) is used to classify the bonding nature. Generally, a covalent bond or open-shell interaction is indicated by ρ(r) > 0.20 au and $\nabla^2\rho$(r) < 0, while an ionic bond or closed-shell interaction exhibits ρ(r) < 0.10 au and $\nabla^2\rho$(r) > 0.[76] A total energy density [H(r)] at the BCP of less than 0 indicates the significant electron-sharing, with the magnitude of H(r) reflecting the degree of bond covalency. The ρ(r), $\nabla^2\rho$(r), and H(r) values at the BCPs for IC1^{I}, TS1^{I} and INT1^{I} of pathway I are in Table 1. The N2-H1 bonding interaction gradually changes from open- to closed-shell, while the O_{yl1}-H1 bond concurrently transforms from closed- to open-shell. The values of H(r) at the N2-H1 and O_{yl1}-H1 BCPs for IC1^{I}, TS1^{I} and INT1^{I} also reflect this bonding evolution.

Values of ρ(r) and $\nabla^2\rho$(r) for other complexes and processes on pathways I, II and III are in Tables S2-S4. Mayer bond orders (MBOs) (Table 1 and Tables S2-S4) for structures on all three pathways similarly reveal dissociation of N-H and formation of the O_{yl1}-H bonds via the TSs.

Table 1 Electron density [ρ(r), au], Laplacian [$\nabla^2\rho$(r), au], total energy density [H(r), au], and MBO of the N2-H1 and O_{yl1}-H1 bonds for $IC1^I$, $TS1^I$ and $INT1^I$ of pathway I.

	Bond	ρ(r)	$\nabla^2\rho$(r)	H(r)	MBO
$IC1^I$	N2-H1	0.287	-1.400	-0.388	0.558
	O_{yl1}-H1	0.048	0.150	-0.002	0.183
$TS1^I$	N2-H1	0.129	-0.072	-0.081	0.340
	O_{yl1}-H1	0.181	-0.429	-0.188	0.335
$INT1^I$	N2-H1	0.050	0.125	-0.004	0.247
	O_{yl1}-H1	0.279	-1.285	-0.383	0.469

LMOs. LMO analysis also reveals bond characteristics and reaction mechanisms.[77, 78] LMO diagrams in Fig. 7 for structures on pathway I show that the N2-H1 σ bond is broken while the O_{yl1}-H1 σ bond is formed from $IC1^I$ to $INT1^I$, in accord with MBO and QTAIM. Also revealed is formation of the N2-H_w σ bond coincident with breaking the O_w-H_w σ bond from $IC3^I$ to $INT3^I$. In the second stage, N2-H1 retains σ bond character, while the N1-H2 σ bond is disrupted from $IC4^I$ to $TS4^I$; the O_{yl1}-H1 σ and N1-H2 σ bonds form from $TS4^I$ to $INT4^I$. The results also reveal that dissociation of the N1-H2 σ bond promotes interaction of H1 and O_{yl1} in water-mediated proton transfer in the second stage. The composition of LMOs (Table S5) indicates that the new O_{yl1}-H1 σ bonds in $INT1^I$ and $INT4^I$ are primarily composed of O_{yl1} 2p and H1 1s orbitals. The LMOs of structures on pathways II and III in Figs. S17 and S18 and corresponding compositions in Tables S6 and S7 also reveal the new O_{yl1}-H σ bonds primarily composed of O_{yl1} 2p and H 1s.

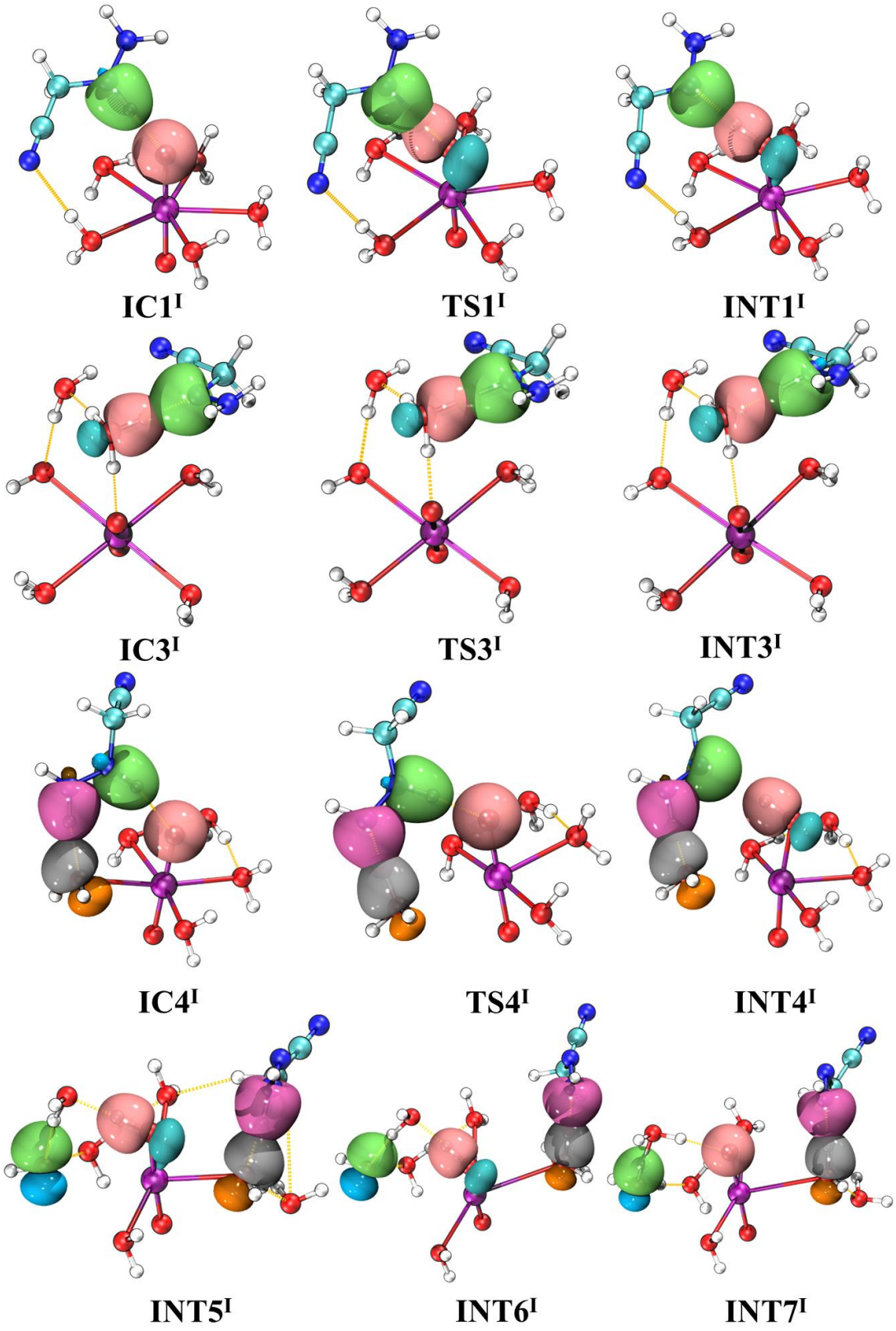

Fig. 7 Diagrams of LMOs (isovalue = 0.08) for structures on pathway I. Yellow dashed lines represent H-bonds; Purple, red, blue, cyan, white balls represent Np, O, N, C, H atoms, respectively.

Spin density. Spin density is used to illuminate the change of oxidation stage of Np, as reported by Gorantla and Mallik.[79] Diagrams of spin density and the value of spin density located on the Np atom for the structures on the pathway I are shown in Fig. 8 and the corresponding values on the Np, O, and N atoms are listed in Table S8. It can be seen from Fig. 8 and Table S8 that the value of the spin density on the Np atom for the structures from $IC1^I$ to $INT3^I$ of the first stage of pathway I is about 2.23 ~ 2.27 a.u., revealing that the oxidation state of Np is Np(V). Moreover, the values of the spin density located on N atoms suggest that the $NCCH_2N_2H_3$ has a radical character. These results indicate that the first Np(VI) is reduced to Np(V) as soon as the $NCCH_2N_2H_3$ binds to the Np(VI) ion. Thus, the first reduction of Np(VI) is the outer-sphere electron transfer from $NCCH_2N_2H_3$ to neptunyl ion in the formation of $IC1^I$, which is supported by previous works.[80-82] As for the structures of the second stage of pathway I, the spin density of Np atom obviously increases from 1.420 ($IC4^I$) to 2.152 ($TS4^I$) to 2.296 a.u. ($INT4^I$), demonstrating that the oxidation state of Np is changed from +VI ($IC4^I$) to +V ($INT4^I$), and this process is achieved by the hydrogen transfer. Therefore, the reduction of the first Np(VI) ion is accompanied with the formation of $IC1^I$, which is the outer-sphere electron transfer. The second Np(VI) ion is reduced from $IC4^I$ to $INT4^I$, which is the hydrogen transfer. The reductions of Np(VI) ions for pathways II and III are similar processes to those of pathway I as presented in Figs. S19-S20 and Tables S9-S10.

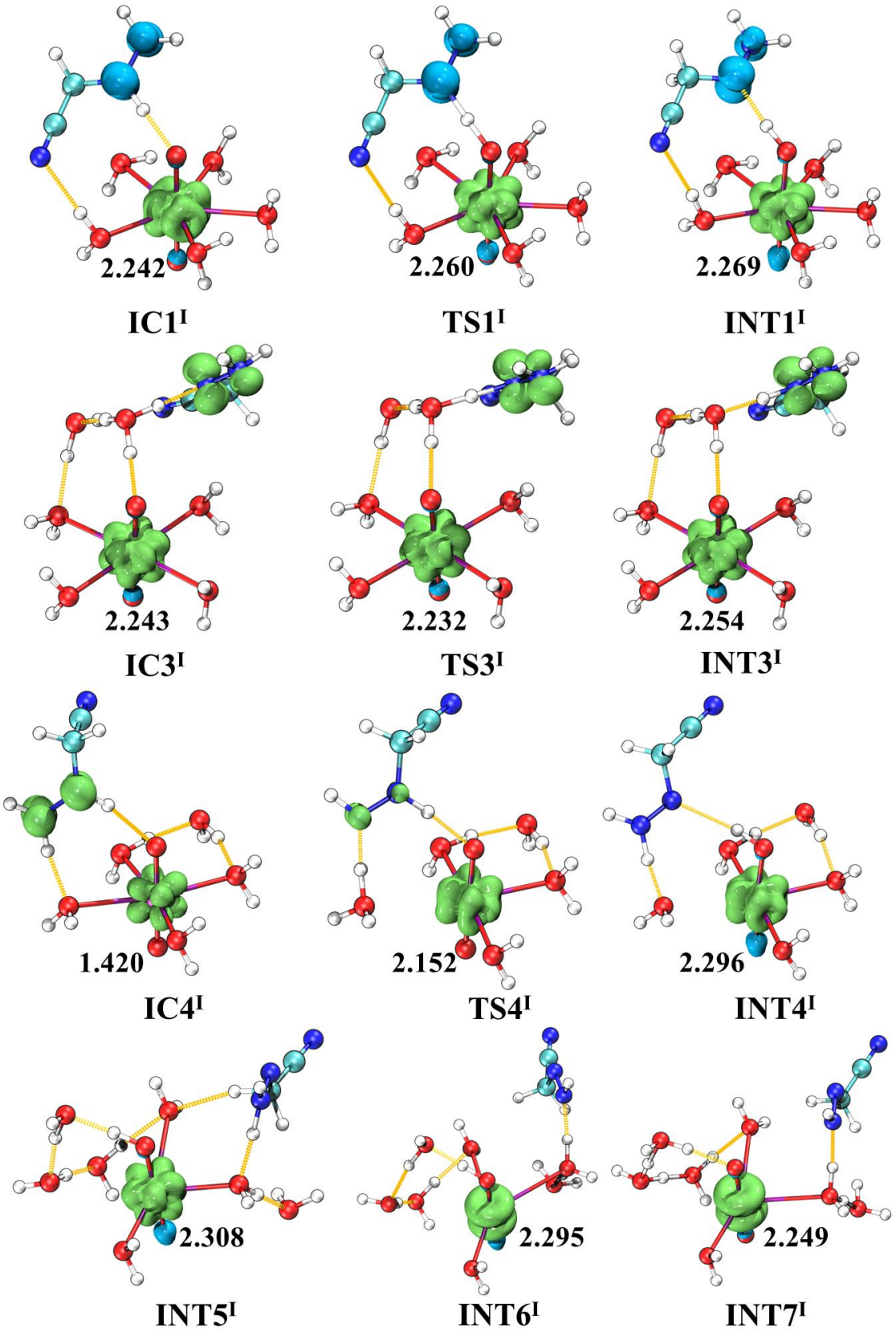

Fig. 8 Diagrams of spin density (isovalue = 0.02) and the value of the spin density on the Np atom for the structures of pathway I.

Conclusion

The PEPs and associated structures for reduction of Np(VI) by HzPn were investigated using scalar-relativistic DFT calculations. We obtained three pathways for free radical ion mechanism via $[NCCH_2N_2H_3]^{+\bullet}$ and formation/dissociation of an O_{yl}-H bond, with the different pathways corresponding to three hydrazine H atoms of the HzPn reductant. Pathway I, the identified optimal route, proceeds by water-mediated proton transfer, with the second stage rate-determining based on PEPs energy barriers. IRC calculations reflect structural transformations from ICs to INTs. Besides, HzPn has a faster kinetics than most other hydrazine derivatives,[42, 43] probably due to σ-π hyperconjugation effect, which obtains that allylhydrazine ($CH_2CHCH_2N_2H_3$) or prop-2-ynylhydrazine ($CHCCH_2N_2H_3$) may holds similar or better reduction ability for Np(VI). Results of QTAIM, MBOs, and LMOs are in accord with expected dissociation and formation of bonds along the reaction pathway. The results of the spin density reveal that the first Np(VI) ion is reduced in the process of the formation of IC1, which is the outer-sphere electron transfer. The reduction of second Np(VI) ion is reduced from $IC4^I$ to $INT4^I$, which is the hydrogen transfer. This work reveals that both water-mediated proton transfer and the σ-π hyperconjugation effect of the hydrazine derivatives can low reduce energy barriers, which provides a theoretical basis for designing potentially more efficient Np(VI) reductants applied of Np/U and Np/Pu in spent fuel reprocessing.

Data availability

Diagrams of spin density for pathways II and III and the corresponding values on the Np, O, and N atoms for pathways I-III; electronic energies for the pathway first stages; $\rho(r)$, $\nabla^2\rho(r)$, H(r), and MBOs of N-H and O_{yl1}-H bonds; optimized geometries and bond distances of ICs and INTs for pathways II and III; diagrams and main atomic orbital composition of LMOs; IRC results; coordinates for all structures are available in the ESI.

Author contributions

Xiao-Bo Li and Qun-Yan Wu performed data curation, visualization, writing-original

draft. Cong-Zhi Wang and Jian-Hui Lan performed formal analysis. Meng Zhang, John K. Gibson, Zhi-Fang Chai and Wei-Qun Shi reviewed and edited the paper. All authors discussed the results of the manuscript.

Conflicts of interest

There are no conflicts to declare.

Acknowledgments

The authors thank Prof. Han-Shi Hu in Tsinghua University for ongoing useful discussions. This work was supported by the National Natural Science Foundation of China (Grant Nos. U1867205, 22076188, 11875058, 21876035), the National Science Fund for Distinguished Young Scholars (21925603). The work of John K. Gibson was supported by the U.S. Department of Energy, Basic Energy Sciences, Heavy Element Chemistry at LBNL under contract NO. DEAC02-05CH11231.

Notes and references

1 Z. Yoshida, S. G. Johnson, T. Kimura and J. R. Krsul, *The Chemistry of the Actinide and Transactinide Elements*, Springer Netherlands, Dordrecht, 2006, pp. 699-812.

2 P. D. Wilson, *The Nuclear Fuel Cycle: From Ore to Waste*, Oxford University Press, United Kingdom, 1996.

3 R. J. Taylor, C. R. Gregson, M. J. Carrott, C. Mason and M. J. Sarsfield, *Solvent Extr. Ion Exc.*, 2013, **31**, 442-462.

4 V. S. Koltunov, R. J. Taylor, S. M. Baranov, E. A. Mezhov, V. G. Pastuschak and I. May, *Radiochim. Acta*, 2000, **88**, 65-70.

5 V. S. Koltunov, E. A. Mezhov and S. M. Baranov, *Radiochemistry*, 2001, **43**, 342-345.

6 V. S. Koltunov, V. I. Marchenko, G. I. Zhuravleva and O. A. Savilova, *Radiochemistry*, 2001, **43**, 334-337.

7 G. Uchiyama, S. Fujine, S. Hotoku and M. Maeda, *Nucl. Technol.*, 1993, **102**, 341-352.

8 G. Uchiyama, S. Hotoku, S. Fujine and M. Maeda, *Nucl. Technol.*, 1998, **122**, 222-227.

9 G. Uchiyama, S. Hotoku, S. Fujine and M. Maeda, *Solvent Extr. Ion Exc.*, 1997, **15**, 863-877.

10 V. S. Koltunov, R. J. Taylor, S. M. Baranov, E. A. Mezhov and I. May, *Radiochim. Acta*, 1999, **86**, 115-121.

11 V. S. Koltunov and S. M. Baranov, *Radiochemistry*, 2000, **42**, 236-241.

12 A. Y. Zhang, J. X. Hu, X. Y. Zhang and F. D. Wang, *J. Radioanal. Nucl. Chem.*, 2002, **253**, 107-113.

13 V. I. Marchenko, K. N. Dvoeglazov, O. A. Savilova and V. I. Volk, *Radiochemistry*, 2012, **54**, 459-464.

14 H. Zhang, G. A. Ye, H. F. Cong, L. Li, H. Yang, G. L. Li, W. F. Zheng, D. X. Jiang, X. C. Liu, S. T. Xiao and T. Lan, *Radiochim. Acta*, 2012, **100**, 813-820.

15 Z. W. Zhu, J. Y. He, Z. F. Zhang, Y. Zhang, J. M. Zhu and W. F. Zhen, *J. Radioanal. Nucl. Chem.*,

2005, **262**, 707-711.

16 T. H. Yan, W. F. Zheng, C. Zuo, L. Xian, Y. Zhang, X. Y. Bian, R. X. Li and Y. Di, *Radiochim. Acta*, 2010, **98**, 35-38.

17 R. J. Taylor, I. May, A. L. Wallwork, I. S. Denniss, N. J. Hill, B. Y. Galkin, B. Y. Zilberman and Y. S. Fedorov, *J. Alloy Compd.*, 1998, **271**, 534-537.

18 R. J. Taylor and I. May, *Czech. J. Phys.*, 1999, **49**, 617-621.

19 D. Y. Chung and E. H. Lee, *B Korean Chem. Soc.*, 2005, **26**, 1692-1694.

20 B. S. Matteson, Doctor of Philosophy, Oregon State University, 2010.

21 V. S. Koltunov and S. M. Baranov, *Inorg. Chem. Acta*, 1987, **140**, 31-34.

22 R. J. Taylor, I. May, V. S. Koltunov, S. M. Baranov, V. I. Marchenko, E. A. Mezhov, V. G. Pastuschak, G. I. Zhuravleva and O. A. Savilova, *Radiochim. Acta*, 1998, **81**, 149-156.

23 V. Koltunov, *J. Nucl. Sci. Technol.*, 2002, **39**, 347-350.

24 Y. Ban, T. Asakura and Y. Morita, *J. Radioanal. Nucl. Chem.*, 2009, **279**, 423-429.

25 V. I. Volk, V. I. Marchenko, K. N. Dvoeglazov, V. N. Alekseenko, S. I. Bychkov, E. Y. Pavlyukevich, V. V. Bondin and A. S. D'yachenko, *Radiochemistry*, 2012, **54**, 143-148.

26 V. I. Marchenko, V. N. Alekseenko and K. N. Dvoeglazov, *Radiochemistry*, 2015, **57**, 366-377.

27 O. A. Zavalina, K. N. Dvoeglazov, E. Y. Pavlyukevich and S. I. Stepanov, *Radiochemistry*, 2017, **59**, 453-457.

28 V. P. Shilov and A. M. Fedoseev, *Radiochemistry*, 2019, **61**, 309-311.

29 K. J. Carr, D. L. Davies, S. A. Macgregor, K. Singh and B. Villa-Marcos, *Chem. Sci.*, 2014, **5**, 2340-2346.

30 B. Zhu, W. Guan, L. K. Yan and Z. M. Su, *J. Am. Chem. Soc.*, 2016, **138**, 11069-11072.

31 H. Y. Zhang, Z. X. Cao, W. Wu and Y. R. Mo, *Angew. Chem., Int. Ed.*, 2018, **57**, 13076-13081.

32 B. E. Haines, J. Q. Yu and D. G. Musaev, *Chem. Sci.*, 2018, **9**, 1144-1154.

33 Douglas W. Crandell, S. B. Muñoz, J. M. Smith and M. H. Baik, *Chem. Sci.*, 2018, **9**, 8542-8552.

34 B. M. Gardner, P. A. Cleaves, C. E. Kefalidis, J. Fang, L. Maron, W. Lewis, A. J. Blake and S. T. Liddle, *Chem. Sci.*, 2014, **5**, 2489-2497.

35 W. S. Ren, E. W. Zhou, B. Fang, G. F. Zi, D. C. Fang and M. D. Walter, *Chem. Sci.*, 2014, **5**, 3165-3172.

36 N. Tsoureas, L. Castro, A. F. Kilpatrick, F. G. N. Cloke and L. Maron, *Chem. Sci.*, 2014, **5**, 3777-3788.

37 B. Fang, L. Zhang, G. Hou, G. Zi, D. C. Fang and M. D. Walter, *Chem. Sci.*, 2015, **6**, 4897-4906.

38 L. Zhang, G. H. Hou, G. F. Zi, W. J. Ding and M. D. Walter, *J. Am. Chem. Soc.*, 2016, **138**, 5130-5142.

39 K. C. Mullane, H. Ryu, T. Cheisson, L. N. Grant, J. Y. Park, B. C. Manor, P. J. Carroll, M. H. Baik, D. J. Mindiola and E. J. Schelter, *J. Am. Chem. Soc.*, 2018, **140**, 11335-11340.

40 L. Chatelain, E. Louyriac, I. Douair, E. Lu, F. Tuna, A. J. Wooles, B. M. Gardner, L. Maron and S. T. Liddle, *Nat. Commun.*, 2020, **11**, 337.

41 Z. P. Cheng, Q. Y. Wu, Y. H. Liu, J. H. Lan, C. Z. Wang, Z. F. Chai and W. Q. Shi, *RSC Adv.*, 2016, **6**, 109045-109053.

42 X. B. Li, Q. Y. Wu, C. Z. Wang, J. H. Lan, S. Y. Ning, Y. Z. Wei, Z. F. Chai and W. Q. Shi, *J. Phys. Chem. A*, 2020, **124**, 3720-3729.

43 X. B. Li, Q. Y. Wu, C. Z. Wang, J. H. Lan, M. Zhang, Z. F. Chai and W. Q. Shi, *J. Phys. Chem. A*, 2021, **125**, 6180-6188.

44 M. J. Janik, R. J. Davis and M. Neurock, *J. Am. Chem. Soc.*, 2005, **127**, 5238-5245.
45 L. Gorb and J. Leszczynski, *J. Am. Chem. Soc.*, 1998, **120**, 5024-5032.
46 S. Antonczak, M. F. Ruiz-Lopez and J. L. Rivail, *J. Am. Chem. Soc.*, 1994, **116**, 3912-3921.
47 S. Simon, M. Sodupe and J. Bertran, *Theor. Chem. Acc.*, 2004, **111**, 217-222.
48 A. O. Furmanchuk, O. Isayev, L. Gorb, O. V. Shishkin, D. M. Hovorun and J. Leszczynski, *Phys. Chem. Chem. Phys.*, 2011, **13**, 4311-4317.
49 J. E. Jee, A. Comas-Vives, C. Dinoi, G. Ujaque, R. van Eldik, A. Lledós and R. Poli, *Inorg. Chem.*, 2007, **46**, 4103-4113.
50 G. Kovács, A. Lledós and G. Ujaque, *Organometallics*, 2010, **29**, 3252-3260.
51 L. K. Harper and C. A. Bayse, *J. Inorg. Biochem.*, 2015, **153**, 60-67.
52 M. H. Ho, M. O'Hagan, M. Dupuis, D. L. DuBois, R. M. Bullock, W. J. Shaw and S. Raugei, *Dalton Trans.*, 2015, **44**, 10969-10979.
53 Y. C. Zhuang, D. S. Ye, S. U. Weng and H. H. G. Tsai, *J. Phys. Chem. B*, 2021, **125**, 11893-11906.
54 C. T. Lee, W. T. Yang and R. G. Parr, *Phys. Rev. B*, 1988, **37**, 785-789.
55 A. D. Becke, *J. Chem. Phys.*, 1993, **98**, 5648-5652.
56 M. J. Frisch, G. W. Trucks, H. B. Schlegel, G. E. Scuseria, M. A. Robb, J. R. Cheeseman, G. Scalmani, V. Barone, G. A. Petersson, H. Nakatsuji, X. Li, M. Caricato, A. V. Marenich, J. Bloino, B. G. Janesko, R. Gomperts, B. Mennucci, H. P. Hratchian, J. V. Ortiz, A. F. Izmaylov, J. L. Sonnenberg, D. Williams-Young, F. Ding, F. Lipparini, F. Egidi, J. Goings, B. Peng, A. Petrone, T. Henderson, D. Ranasinghe, V. G. Zakrzewski, J. Gao, N. Rega, G. Zheng, W. Liang, M. Hada, M. Ehara, K. Toyota, R. Fukuda, J. Hasegawa, M. Ishida, T. Nakajima, Y. Honda, O. Kitao, H. Nakai, T. Vreven, K. Throssell, J. A. Montgomery Jr, J. E. Peralta, F. Ogliaro, M. J. Bearpark, J. J. Heyd, E. N. Brothers, K. N. Kudin, V. N. Staroverov, T. A. Keith, R. Kobayashi, J. Normand, K. Raghavachari, A. P. Rendell, J. C. Burant, S. S. Iyengar, J. Tomasi, M. Cossi, J. M. Millam, M. Klene, C. Adamo, R. Cammi, J. W. Ochterski, R. L. Martin, K. Morokuma, O. Farkas, J. B. Foresman and D. J. Fox, Gaussian 16, Revision B.01, Gaussian, Inc., Wallingford CT, 2016.
57 J. P. Dognon, C. Clavaguéra and P. Pyykkö, *Chem. Sci.*, 2012, **3**, 2843-2848.
58 H. S. Hu, Y. H. Qiu, X. G. Xiong, W. H. E. Schwarz and J. Li, *Chem. Sci.*, 2012, **3**, 2786-2796.
59 Q. Y. Wu, J. H. Lan, C. Z. Wang, Y. L. Zhao, Z. F. Chai and W. Q. Shi, *J. Phys. Chem. A*, 2014, **118**, 10273-10280.
60 Q. Y. Wu, C. Z. Wang, J. H. Lan, C. L. Xiao, X. K. Wang, Y. L. Zhao, Z. F. Chai and W. Q. Shi, *Inorg. Chem.*, 2014, **53**, 9607-9614.
61 D. E. Smiles, E. R. Batista, C. H. Booth, D. L. Clark, J. M. Keith, S. A. Kozimor, R. L. Martin, S. G. Minasian, D. K. Shuh, S. C. E. Stieber and T. Tyliszczak, *Chem. Sci.*, 2020, **11**, 2796-2809.
62 W. Küchle, M. Dolg, H. Stoll and H. Preuss, *J. Chem. Phys.*, 1994, **100**, 7535-7542.
63 X. Cao, M. Dolg and H. Stoll, *J. Chem. Phys.*, 2003, **118**, 487-496.
64 X. Cao and M. Dolg, *J. Molec. Struct. (THEOCHEM).* 2004, **673**, 203-209.
65 Q. Y. Wu, J. H. Lan, C. Z. Wang, Y. L. Zhao, Z. F. Chai and W. Q. Shi, *J. Phys. Chem. A*, 2014, **118**, 10273-10280.
66 K. Fukui, *J. Phys. Chem.*, 1970, **74**, 4161-4163.
67 J. Cioslowski and S. T. Mixon, *J. Am. Chem. Soc.*, 1991, **113**, 4142-4145.
68 R. F. W. Bader, *Acc. Chem. Res.*, 1985, **18**, 9-15.
69 J. Pipek and P. G. Mezey, *J. Chem. Phys.*, 1989, **90**, 4916-4926.

70 T. Lu and F. W. Chen, *J. Comput. Chem.*, 2012, **33**, 580-592.

71 S. T. Xiao, G. A. Ye, L. Li, X. C. Liu, H. Yang, H. B. Li and Z. W. Yuan, *J. Radioanal. Nucl. Chem.*, 2017, **311**, 1565-1575.

72 P. Smith, R. D. Stevens and R. A. Kaba, *J. Phys. Chem.*, 1971, **75**, 2048-2055.

73 R. F. W. Bader and H. Essen, *J. Chem. Phys.*, 1984, **80**, 1943-1960.

74 J. Andrés, S. Berski, J. Contreras-García and P. González-Navarrete, *J. Phys. Chem. A*, 2014, **118**, 1663-1672.

75 M. Fugel, A. Dittmer, F. Kleemiss and S. Grabowsky, *J. Phys. Chem. A*, 2021, **125**, 4070-4078.

76 C. F. Matta and R. J. Boyd, *The Quantum Theory of Atoms in Molecules*, Wiley-VCH Verlag GmbH & Co. KGaA, Weinheim, 2007, pp.1-34.

77 Y. Wakatsuki, N. Koga, H. Werner and K. Morokuma, *J. Am. Chem. Soc.*, 1997, **119**, 360-366.

78 R. Z. Sun, M. Y. Yu, G. Q. Luo, X. Li, H. Tian and H. Yao, *Chem. Eng. J*, 2021, **407**, 127113.

79 K. R. Gorantla and B. S. Mallik, *J. Phys. Chem. A*, 2022, **126**, 3301-3310.

80 J. G. Muller, R. P. Hickerson, R. J. Perez and C. J. Burrows, *J. Am. Chem. Soc.*, 1997, **119**, 1501-1506.

81 R. S. Miller, J. M. Sealy, M. Shabangi, M. L. Kuhlman, J. R. Fuchs and R. A. Flowers, *J. Am. Chem. Soc.*, 2000, **122**, 7718-7722.

82 Y.-M. Lee, S. Kim, K. Ohkubo, K.-H. Kim, W. Nam and S. Fukuzumi, *J. Am. Chem. Soc.*, 2019, **141**, 2614-2622.